LETTER

doi:10.1038/nature13073

Inhibition of *miR-25* improves cardiac contractility in the failing heart

Christine Wahlquist[1]*, Dongtak Jeong[2]*, Agustin Rojas-Muñoz[1], Changwon Kho[2], Ahyoung Lee[2], Shinichi Mitsuyama[2], Alain van Mil[1,3], Woo Jin Park[4], Joost P. G. Sluijter[3], Pieter A. F. Doevendans[3], Roger J. Hajjar[2] & Mark Mercola[1]

Heart failure is characterized by a debilitating decline in cardiac function[1], and recent clinical trial results indicate that improving the contractility of heart muscle cells by boosting intracellular calcium handling might be an effective therapy[2,3]. MicroRNAs (miRNAs) are dysregulated in heart failure[4,5] but whether they control contractility or constitute therapeutic targets remains speculative. Using high-throughput functional screening of the human microRNAome, here we identify miRNAs that suppress intracellular calcium handling in heart muscle by interacting with messenger RNA encoding the sarcoplasmic reticulum calcium uptake pump SERCA2a (also known as ATP2A2). Of 875 miRNAs tested, *miR-25* potently delayed calcium uptake kinetics in cardiomyocytes *in vitro* and was upregulated in heart failure, both in mice and humans. Whereas adeno-associated virus 9 (AAV9)-mediated overexpression of *miR-25 in vivo* resulted in a significant loss of contractile function, injection of an antisense oligonucleotide (antagomiR) against *miR-25* markedly halted established heart failure in a mouse model, improving cardiac function and survival relative to a control antagomiR oligonucleotide. These data reveal that increased expression of endogenous *miR-25* contributes to declining cardiac function during heart failure and suggest that it might be targeted therapeutically to restore function.

Heart failure is the culmination of diverse cardiovascular diseases, including hypertension, ischaemic disease and atherosclerosis, valvular insufficiency, myocarditis, and contractile protein mutations, and is uniformly characterized by a progressive loss of contractile function and reserve[1]. The prevailing therapeutic strategy is to block the deleterious effects of the renin–angiotensin and sympathetic systems, but existing drugs target few mechanisms within the failing cardiomyocyte and there is a critical need for novel drugs, especially for treating patients with advanced heart failure[6,7]. A complex intracellular network balances contractility and intracellular Ca^{2+} handling in relation to workload[8]; however, the role of miRNAs in cardiac contractility remains largely unexplored. miRNAs fine tune nearly all normal and pathological processes by downregulating proteins that occupy key nodal points in biological control networks[9,10]. We reasoned that miRNAs that repress contractility[11] might be upregulated during human heart failure, and might therefore constitute novel targets for therapeutic intervention.

The calcium-transporting ATPase SERCA2a is the primary mechanism of Ca^{2+} uptake during excitation–contraction coupling in cardiomyocytes. Impaired Ca^{2+} uptake resulting from decreased expression and reduced activity of SERCA2a is a hallmark of heart failure[2]. Accordingly, restoration of SERCA2a by gene transfer has proven effective in improving key parameters of heart failure in animal models[12] and more recently in clinical trials[3]. Thus, miRNAs that downregulate SERCA2a might be elevated in heart failure and compromise cardiac function. Computational algorithms predict >300 miRNAs that target SERCA2a (miRNA Data Integration Portal[13]), but they are error prone, necessitating empirical evaluation[14]. We therefore functionally screened a whole-genome collection of miRNAs for selective downregulation of the Ca^{2+} pump. To perform the screen, we fused the *SERCA2a* mRNA 3′ untranslated region (UTR) sequence downstream of an enhanced green fluorescent protein (*eGFP*) coding region, making a 'target sensor' construct to permit detection of active miRNAs by a decrease in eGFP fluorescence (Fig. 1a, b). In the primary screen, 144 miRNAs reduced eGFP fluorescence by >30% with $P < 0.05$ (Fig. 1c, d), and 82 were confirmed by testing through a dose range (Fig. 1e, f and Supplementary Table 1). Thirty-two were evolutionarily conserved and 15 were both evolutionarily conserved and reported to be upregulated in human heart failure (see Methods) (Fig. 1e). Four caused a highly significant ($P < 0.001$, one-tailed analysis of variance (ANOVA)) prolongation of the decay phase of the Ca^{2+} transient in the cardiomyocyte HL-1 cell line, shown here as the duration from 75% to 25% maximal value, $CaTD_{75-25}$ (Fig. 1g), measured using an automated platform[15]. The most potent miRNA was *miR-25*, which elicited a physiological effect comparable to that of the short interfering RNA (siRNA) directed against SERCA2a, *siSERCA2a* (Fig. 1h). We confirmed that *miR-25* is upregulated in human myocardial samples from patients with severe heart failure (Fig. 1i). *In situ* hybridization revealed that *miR-25* is expressed primarily in cardiomyocytes of trans-aortic constriction (TAC)-induced failing mouse hearts, with no detectable expression in cardiac fibroblasts or vascular endothelial cells, and low expression in vascular smooth muscle (Fig. 2).

To establish a link between *miR-25* and cardiac function, we identified putative protein targets involved in Ca^{2+} handling computationally (DianaLab miRPath with TargetScan Mouse v.5.0, see Methods). In addition to SERCA2a, these included inositol-1,4,5-trisphosphate receptor 1 (IP3R1), which was selectively downregulated by *miR-25* transient transfection in HL-1 cells (Fig. 3a and Extended Data Fig. 1a). Other candidate proteins involved in calcium handling, including the sodium–calcium exchanger (NCX1; also known as SLC8A1), calmodulin kinase 2 (CaMKII), phospholamban (PLN) and calmodulin 3 (CALM3) were unaffected in HL-1 cells transfected with *miR-25* (Extended Data Fig. 2). miRNAs bind cognate mRNAs by imprecise base pairing to specific recognition elements[9,10]. Single putative *miR-25* recognition sites were identified within *SERCA2a* and *IP3R1* 3′ UTR sequences by TargetScan Human v.6.2 (Fig. 3b and Extended Data Fig. 1b). Mutation of these sequences abolished the ability of *miR-25* to inhibit reporter expression (Fig. 3b and Extended Data Fig. 1b), further supporting selective *miR-25* interactions with the mRNAs, and indicating that the single recognition elements identified in the 3′ UTRs of the *SERCA2a* and *IP3R1* mRNAs are sufficient for *miR-25* activity.

Having shown that *miR-25* regulates SERCA2a and IP3R1, we evaluated whether siRNAs directed against these proteins could mimic the effect of *miR-25* on cardiac Ca^{2+} transient kinetics *in vitro*. Transfection of *siSerca2a* significantly slowed the decay (Ca^{2+} re-uptake) phase of the transient ($CaTD_{75-25}$) relative to controls in spontaneously contracting

[1]Department of Bioengineering, University of California, San Diego, and the Muscle Development and Regeneration Program, Sanford-Burnham Medical Research Institute, 10901 North Torrey Pines Road, La Jolla, California 92037, USA. [2]The Cardiovascular Research Center, Icahn School of Medicine at Mount Sinai, New York, New York 10029, USA. [3]Department of Cardiology, University Medical Center Utrecht and ICIN Netherlands Heart Institute, Heidelberglaan 100, room G02.523, 3584 CX Utrecht, The Netherlands. [4]Global Research Laboratory, Gwangju Institute of Science and Technology, 123 Cheomdan-gwagiro, Buk-gu, Gwangju 500-712, South Korea.
*These authors contributed equally to this work.

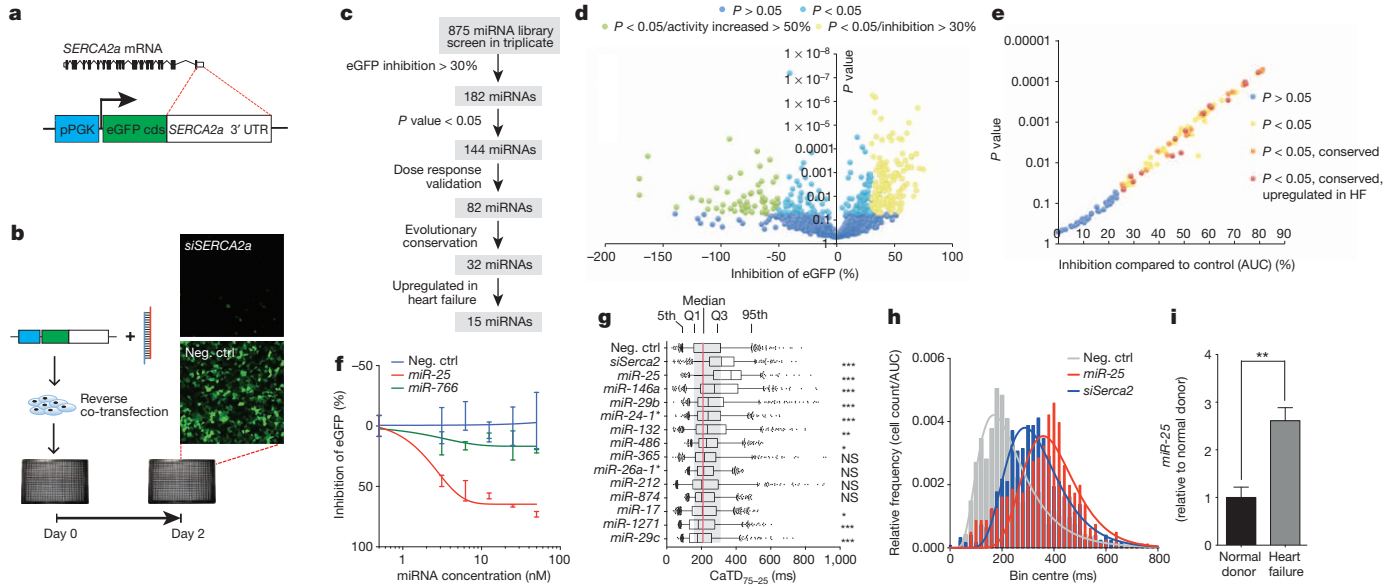

Figure 1 | High-content screening identifies miRNAs that control SERCA2a. **a**, **b**, Target sensor construct (**a**) and screening workflow (**b**). cds, coding DNA sequence; Neg. ctrl, negative control; pPGK, phosphoglycerate kinase promoter. **c**, Screening summary. **d**, **e**, Primary ($n = 3$) (**d**) and confirmatory ($n = 3$) (**e**) screen data plotted as percentage inhibition relative to siRNA against *SERCA2a* (100% inhibition) and scrambled sequence control (0% inhibition) (*x*-axis; AUC, area under the curve) and *P* value from Student's *t*-test (*y*-axis). HF, heart failure. **f**, eGFP–SERCA2a inhibition by *miR-25* and inactive *miR-766* relative to scrambled sequence control ($n = 10$). **g**, Ca^{2+} transient kinetic analysis of HL-1 cells transfected with miRNAs that inhibited eGFP–SERCA2a (panel **e**) and are evolutionarily conserved and upregulated in human heart failure ($n > 550$ cells per group). Box shows 25th to 75th percentiles; whiskers show 5th and 95th percentiles; dots indicate outliers. $^*P < 0.05$, $^{**}P < 0.01$, $^{***}P < 0.001$. NS, not significant (one-tailed ANOVA). **h**, Frequency distribution and log-normal curve fits for $CaTD_{75–25}$ values from panel **f**, normalized to sample size. Both *siSerca2a* and *miR-25* increased $CaTD_{75–25}$ values. **i**, *miR-25* is upregulated in human heart failure samples, as demonstrated by quantitative polymerase chain reaction (qPCR). Data are represented as mean ± standard error of the mean (s.e.m.). $^{**}P < 0.01$ ($n = 5$), Student's *t*-test. All replicates (*n*) are biological. Primary and confirmatory screens were performed once (**d**, **e**); subsequent analyses were performed two (**f**–**h**) or three (**i**) times.

HL-1 cells (Fig. 3c and Extended Data Fig. 1c) and neonatal rat ventricular cardiomyocytes (NRVCs; Extended Data Fig. 1d); however, the maximal velocity of the upstroke phase of the Ca^{2+} transient (V_{max}) was unchanged (Extended Data Fig. 3), accurately reproducing the effect of *miR-25* and mimicking the ~1.5–2-fold decline reported for ventricular cardiomyocytes isolated from failing human hearts[16,17]. siRNA against IP3R1 only minimally affected Ca^{2+} transient kinetics in HL-1 cells and not at all in NRVCs ($CaTD_{50}$, $CaTD_{75–25}$ and V_{max}; Fig. 3c and Extended Data Fig. 3), suggesting that the predominant effect of *miR-25* on Ca^{2+} transient kinetics is mediated through downregulation of SERCA2a.

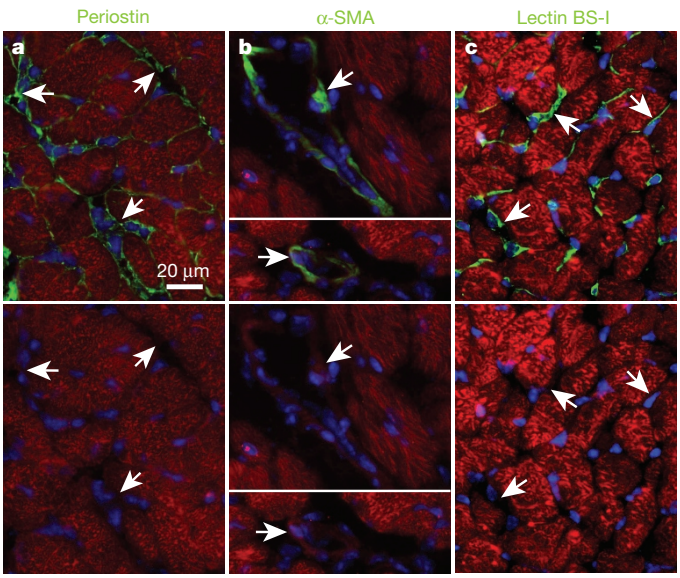

Figure 2 | Endogenous *miR-25* expression in the heart. **a**–**c**, *In situ* hybridization, revealing endogenous *miR-25* expression in failing LV myocardium (red) compared with periostin (**a**, top panel versus bottom panel), α-smooth muscle actin (α-SMA) (**b**) and lectin BS-1 (**c**) staining (each in green). Hoechst 33342 staining marks nuclei (blue). Arrows indicate examples of non-cardiomyocytes. Scale bar, 20 μm. Data are representative of two biological replicates.

We evaluated the physiological effect of blocking *miR-25*. AntagomiRs are antisense oligonucleotides modified to enhance duplex stability and have been used effectively to inhibit miRNA function *in vitro* and *in vivo*[18]. Anti-*miR-25* transfection alone decreased $CaTD_{75–25}$ in HL-1 cells but had no effect in NRVCs (Fig. 3c and Extended Data Fig. 1d). Importantly, when co-transfected, anti-*miR-25* cancelled the prolonging effect of *miR-25* on $CaTD_{75–25}$, restoring kinetic parameters to near normal in both cell types.

We next assessed the physiological consequences of administering *miR-25* and anti-*miR-25 in vivo*. AAV9-mediated gene transfer of *miR-25* increased the levels of *miR-25* by approximately 50% and correspondingly decreased SERCA2a levels in ventricular myocardium (Fig. 3d–f), causing a progressive decline in fractional shortening, an index of cardiac function (Fig. 3g, h). Haemodynamic analyses at the termination of the studies (6 weeks after AAV transfer) confirmed that left ventricular (LV) function had declined in *miR-25*-injected mice (Fig. 3i–k and Extended Data Fig. 4b, c). By contrast, AAV-mediated transfer of *miR-92a* (Fig. 3d, e), which has the same seed sequence (AUUGCAC) as *miR-25*, did not affect SERCA2a levels (Fig. 3f) or significantly affect LV function (Fig. 3g–k and Extended Data Fig. 4b, c), although it downregulated integrin α5, a target involved in angiogenesis[19] (Extended Data Fig. 4a), despite the identical copy number of integrated AAV genomes (Extended Data Fig. 5). Together, these results point to a selective interaction between *miR-25* and *Serca2a* mRNA that is consistent with the importance of non-seed sequences for target specificity[20], and also indicate that elevated *miR-25* can depress cardiac function. To

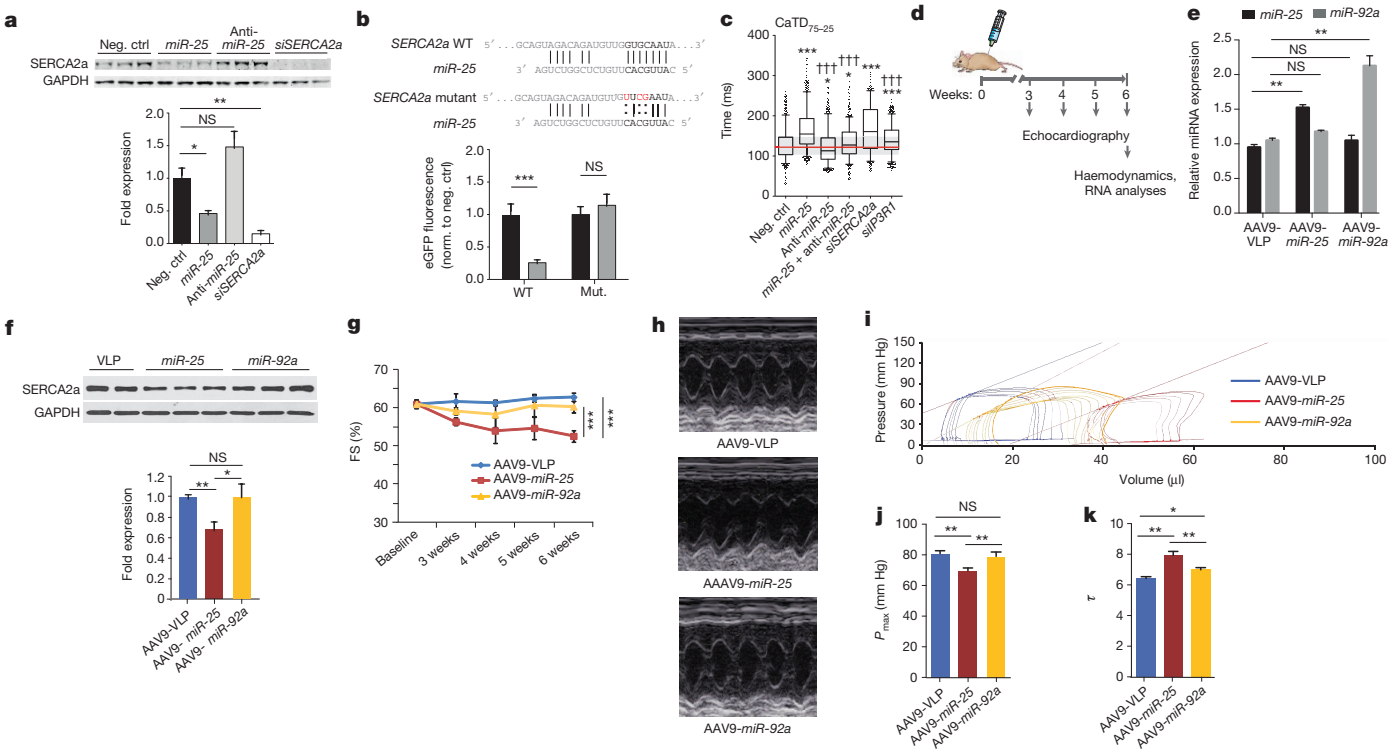

Figure 3 | *miR-25* directly targets SERCA2a and regulates contractile Ca^{2+} kinetics. **a**, Effects of *miR-25*, anti-*miR-25* and controls (scrambled sequence and *Serca2a* siRNA) on SERCA2a protein levels. **b**, Mutagenesis of the putative *mir-25* recognition element in the *SERCA2a* mRNA 3′ UTR abolished inhibition by *miR-25*. $*P < 0.05$, $**P < 0.01$ ($n = 10$; Student's *t*-test), compared with control. Mut., mutant; Norm., normalized; WT, wild type. **c**, Anti-*miR-25* diminished the effect of *miR-25* on $CaTD_{75–25}$ in transfected HL-1 cells. siRNA against IP3R1 had a minimal effect. Extended Data Fig. 3 shows additional parameters and similar results using NRVCs. Box plots as in Fig. 1g. *, † indicate significant differences (* or $†P < 0.05$, ** or $††P < 0.01$, *** or $†††P < 0.001$, one-tailed ANOVA) from negative control (*) or *miR-25* (†) ($n > 550$ cells per group). The data in panels **a**–**c** represent one of three independent experiments. **d**, Protocol for AAV9-mediated cardiac gene transfer. **e**, AAV-*miR-25* ($n = 4$) and AAV-*miR-92a* ($n = 5$) increased levels of their respective miRNAs relative to AAV-VLP control ($n = 3$). **f**, **g**, *miR-25*, but not *miR-92a*, diminished SERCA2a protein levels (**f**) and fractional shortening (FS; percentage) after injection ($n = 5$ for each cohort; **g**). **h**, LV M-mode images. **i**–**k**, Pronounced effect of *miR-25* on pressure–volume relationship (**i**) and P_{max} (**j**) showing decreased function relative to *miR-92a* and control AAV9; and the effect on τ, the time constant for LV relaxation, suggestive of diastolic dysfunction ($n = 5$, AAV9-VLP; $n = 4$, AAV9-*miR-25*; $n = 5$, AAV9-*miR-92a*). Data are represented as mean ± s.e.m. in all panels except **c**. NS, not significant. All replicates (*n*) are biological.

evaluate the selectivity and efficacy of anti-*miR-25*, we intravenously injected anti-miRNAs formulated with *in vivo*-jetPEI reagent mixture. Anti-*miR-25* injection decreased endogenous *miR-25* levels in LV myocardium of both wild-type and SERCA2a knockout mice relative to treatment with a control (scrambled sequence) anti-miR (Extended Data Fig. 6a), but did not affect *miR-92a* (Extended Data Fig. 7). Accordingly, anti-*miR-25* increased SERCA2a levels as expected in wild-type mice (Extended Data Fig. 6b). Notably, however, anti-*miR-25* did not improve the cardiac morphometric or haemodynamic parameters of SERCA2a knockout mice (Extended Data Fig. 8), suggesting that the Ca^{2+} pump is a critical target for *miR-25*.

Because *miR-25* decreased SERCA2a levels *in vitro* and *in vivo*, we evaluated whether administration of anti-*miR-25* would affect cardiac function during chronic heart failure. Mice were subjected to 3 months of TAC to chronically increase LV load and cause LV dilation before administering anti-*miR-25*. Once heart failure was established, anti-*miR-25* or a control anti-miRNA were injected intravenously and the mice were subsequently monitored for their effects on heart function (Fig. 4a). Echocardiography revealed substantial improvements in cardiac function after injection of anti-*miR-25* at 4.5 and 5.5 months after TAC, despite constant pressure overload, compared with severe deterioration in animals injected with the control anti-miRNA (Fig. 4b, c and Supplementary Table 2). Furthermore, haemodynamic analyses at the termination of the studies (5.5 months after TAC) showed substantially improved LV function in the anti-*miR-25*-injected mice, with the treatment effectively restoring the load-independent parameter end systolic pressure volume relationship (ESPVR) and the ejection fraction (EF) to normal levels (Fig. 4d–f and Supplementary Table 3). The heart weight to body weight ratio was also stabilized (Fig. 4g). Survival of the TAC-induced heart failure animals was also improved, with 7/8 anti-*miR-25*-injected and 8/8 sham-operated animals surviving versus 7/22 of the control anti-miRNA-injected animals (Kaplan–Meier analysis, Extended Data Fig. 9), reflected by an increased probability of survival of TAC animals injected with anti-*miR-25* versus control anti-miRNA ($P = 0.0131$, log-rank test). Consistent with improved cardiac function, anti-*miR-25*-injected mice had significantly reduced levels of endogenous *miR-25* compared with control animals (both TAC (Fig. 4h) and sham-operated (Extended Data Fig. 6a)). Neither anti-*miR-25* nor the control anti-miRNA affected the cardiac physiology of sham-operated animals (Extended Data Fig. 8). Total and SUMOylated SERCA2a levels were significantly increased (Fig. 4i and Extended Data Fig. 10), indicating that anti-*miR-25* injection restored the loss of SERCA2a protein as well as post-translational modifications of SERCA2a such as SUMOylation (which improves transporter stability and ATPase activity[21]) despite the prior onset of heart failure. Furthermore, injection of anti-*miR-25* reduced fibrosis (Fig. 4j–l, n–p, r–t, v) and also normalized cardiomyocyte cell size (Fig. 4m, q, u, w). Given that anti-*miR-25* had no salutary effect on cardiac morphometric or haemodynamic parameters in SERCA2a knockout mice (Extended Data Fig. 8), did not affect expression of other miRNAs with homologous seed sequences (Extended Data Fig. 7), and that AAV9-mediated cardiac transfer of *miR-25* selectively affected SERCA2a (Fig. 3f), we propose that the

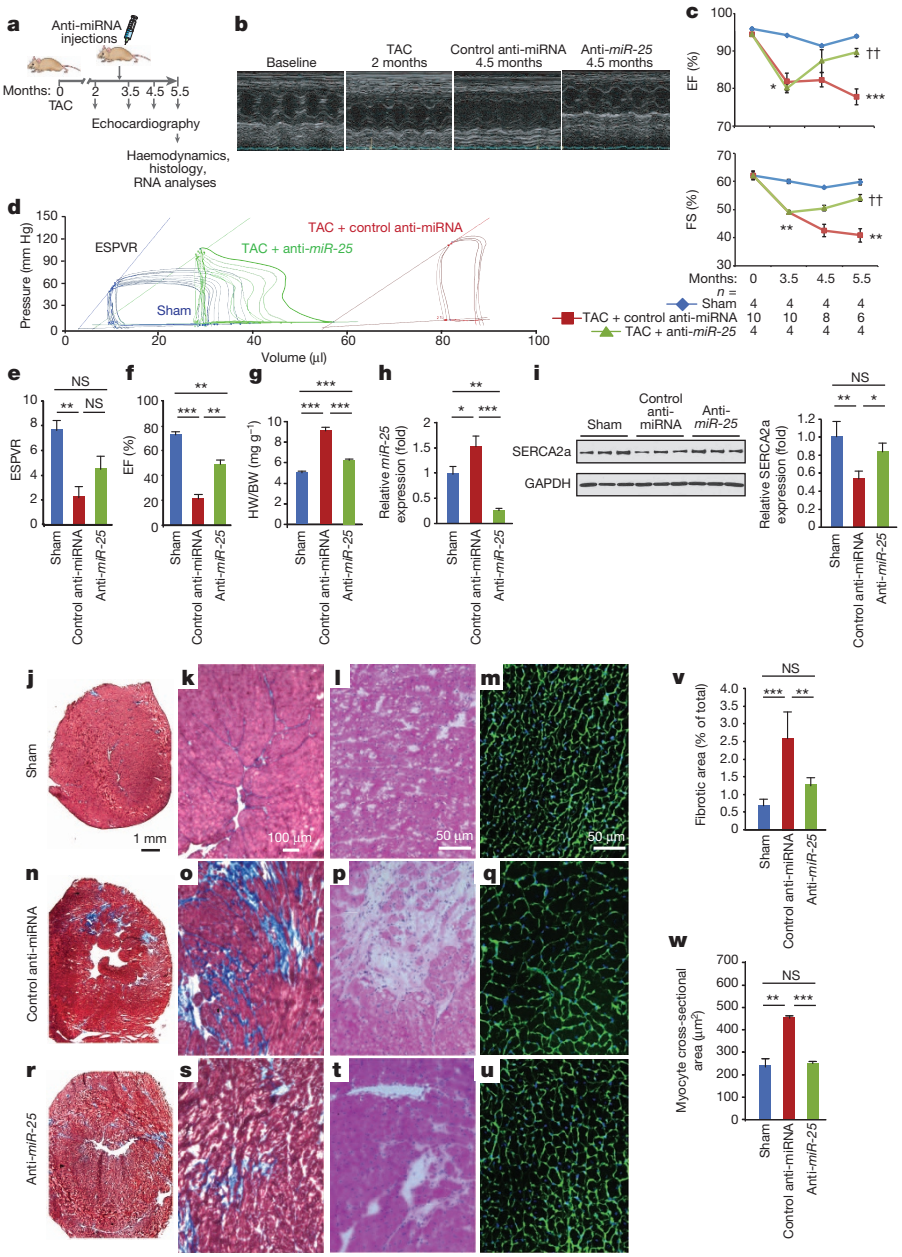

Figure 4 | Inhibition of *miR-25* normalizes TAC-induced cardiac dysfunction. **a**, Protocol for anti-*miR-25* therapy in the mouse TAC heart failure model. **b**, LV M-mode images showing dilation with control anti-miRNA in contrast with anti-*miR-25* injected mice. **c**, Effect on echocardiographic indices of LV function: EF and fractional shortening (FS), expressed as percentages. The number of animals initiated is $n = 4$ (sham operated), 10 (TAC plus control anti-miRNA) and 4 (TAC plus anti-*miR-25*); the numbers analysed per time point are indicated and reflect deaths in the TAC plus control anti-miRNA group. **d**–**f**, Haemodynamic effects. **d**, Pressure–volume plots of treatment cohorts as indicated. Note anti-*miR-25* trend towards normalization of haemodynamic indices of end ESPVR (slope of lines in **d**, **e**), and EF (**f**). $n = 4$ (sham operated), 4 (TAC plus control anti-miRNA) and 3 (TAC plus anti-*miR-25*). **g**, Heart weight (HW) to body weight (BW) ratio. $n = 5$ (sham), 8 (TAC plus control anti-miRNA) and 4 (TAC plus anti-*miR-25*). **h**, **i**, Effect of treatment on endogenous *miR-25* levels (**h**; qPCR, $n = 4$) and SERCA2a protein (**i**; immunoblotting, $n = 3$). **j**–**u**, Masson's trichrome (**j**, **k**, **n**, **o**, **r**, **s**), haematoxylin/eosin (**l**, **p**, **t**) and wheat germ agglutinin (WGA) (**m**, **q**, **u**) stained sections of hearts and LV wall. **v**, Quantified fibrotic area ($n = 3$ (sham operated), 4 (TAC plus control anti-miRNA) and 5 (TAC plus anti-*miR-25*)). **w**, Average cardiomyocyte cross-sectional area ($n = 3$ for all cohorts). For all panels, mean ± s.e.m. *, † indicate significant differences (* or †$P < 0.05$, ** or ††$P < 0.01$, *** or †††$P < 0.001$, Student's *t*-test between sham and anti-miRNA (*) or control anti-miRNA and anti-*miR-25* (†)). NS, not significant. All replicates (*n*) are biological and represent one of two independent experiments.

beneficial effect of anti-*miR-25* is due to the inhibition of pathologically upregulated endogenous *miR-25* and the subsequent restoration of SERCA2a activity. To our knowledge, these data provide the first evidence that cardiac delivery of an anti-miRNA can directly control SERCA2a protein levels to achieve a long-term improvement in cardiac function.

These studies identified *miR-25* as a critical repressor of SERCA2a and cardiac function during heart failure. Of note, several mechanisms beyond SERCA2a deficiency, such as changes in K^+ channel density, NCX expression and myofilament sensitivity to Ca^{2+}, also contribute to slowing of the Ca^{2+} transient in advanced heart failure[22]. *miR-25* might also control IP3R1, and thus could be involved under conditions of inositol-1,4,5-trisphosphate sensitization, such as in response to endothelin 1, angiotensin and phenylephrine[23] or in local Ca^{2+} control[24]. NADPH oxidase 4 (NOX4) was recently shown to be downregulated

by *miR-25* in a mouse model of diabetic nephropathy[25]; however, NOX4 levels did not change significantly in our long-term TAC heart failure model (data not shown). Whether NOX4, which is responsible for the production of superoxide, might contribute to the salutary effects of anti-*miR-25* therapy is unclear as it is reported to confer both protective and detrimental effects[26]. Finally, *miR-25* was recently reported to decrease acutely after aortic constriction in mice[27], in contrast with the chronic elevation reported here and in human heart failure samples, perhaps reflecting the very different stages of pathogenesis. In conclusion, our data suggest that inhibition of *miR-25* may be a novel therapeutic strategy for the treatment of heart failure.

METHODS SUMMARY

For primary screening, HEK293 cells were co-transfected with the Ambion Pre-miR miRNA Precursor Human v.2.0 microRNA library (25 nM) and 300 ng *SERCA2a* 3′ UTR target sensor plasmid (Fig. 1a) per well in 384-well plates, in triplicate.

For secondary screening, Ca^{2+} transient recordings (10 s, 33 frames per second) were acquired from HL-1 cardiomyocytes and NRVCs transfected with candidate miRNAs and loaded with Hoechst 33342 and Fluo-4 72 h after transfection, and analysed to derive cytoplasmic calcium transient kinetic parameters using a KIC instrument and software (Vala Sciences). Unresponsive or low responding cells were removed by gating. Statistical significance was determined using one-way ANOVA.

All mice were housed and treated in accordance with guidelines from the National Institutes of Health and institutional animal care and use committees, and protocols were approved by the Mount Sinai School of Medicine or Sanford-Burnham Medical Research Institute animal care and use committees.

LV samples were from explanted hearts of patients with severe heart failure, obtained at the time of cardiac transplantation. Non-failing hearts (controls) were from patients who died of cerebrovascular accidents with no evidence of contractile dysfunction by echocardiography. The 5 non-failing hearts (3 males and 2 females) had a median age of 43. The 5 heart-failure patients (4 males and 1 female) had a median age of 54 and their mean EF before cardiac transplantation was 22 ± 3%.

Online Content Any additional Methods, Extended Data display items and Source Data are available in the online version of the paper; references unique to these sections appear only in the online paper.

Received 1 January 2013; accepted 23 January 2014.
Published online 12 March 2014.

1. Bonow, R. O., Mann, D. L., Zipes, D. P. & Libby, P. *Braunwald's Heart Disease* (Saunders, 2011).
2. Meyer, M. *et al.* Alterations of sarcoplasmic reticulum proteins in failing human dilated cardiomyopathy. *Circulation* **92,** 778–784 (1995).
3. Jessup, M. *et al.* Calcium upregulation by percutaneous administration of gene therapy in cardiac disease (CUPID): a phase 2 trial of intracoronary gene therapy of sarcoplasmic reticulum Ca^{2+}-ATPase in patients with advanced heart failure. *Circulation* **124,** 304–313 (2011).
4. Ikeda, S. *et al.* Altered microRNA expression in human heart disease. *Physiol. Genomics* **31,** 367–373 (2007).
5. Leptidis, S. *et al.* A deep sequencing approach to uncover the miRNOME in the human heart. *PLoS ONE* **8,** e57800 (2013).
6. Shah, A. M. & Mann, D. L. In search of new therapeutic targets and strategies for heart failure: recent advances in basic science. *Lancet* **378,** 704–712 (2011).
7. Mudd, J. O. & Kass, D. A. Tackling heart failure in the twenty-first century. *Nature* **451,** 919–928 (2008).
8. Greenstein, J. L. & Winslow, R. L. Integrative systems models of cardiac excitation–contraction coupling. *Circ. Res.* **108,** 70–84 (2011).
9. Bartel, D. P. MicroRNAs: target recognition and regulatory functions. *Cell* **136,** 215–233 (2009).
10. Filipowicz, W., Bhattacharyya, S. N. & Sonenberg, N. Mechanisms of post-transcriptional regulation by microRNAs: are the answers in sight? *Nature Rev. Genet.* **9,** 102–114 (2008).
11. Gurha, P. *et al.* Targeted deletion of microRNA-22 promotes stress-induced cardiac dilation and contractile dysfunction. *Circulation* **125,** 2751–2761 (2012).
12. Kawase, Y. *et al.* Reversal of cardiac dysfunction after long-term expression of SERCA2a by gene transfer in a pre-clinical model of heart failure. *J. Am. Coll. Cardiol.* **51,** 1112–1119 (2008).
13. Shirdel, E. A., Xie, W., Mak, T. W. & Jurisica, I. NAViGaTing the micronome—using multiple microRNA prediction databases to identify signalling pathway-associated microRNAs. *PLoS ONE* **6,** e17429 (2011).
14. Lemons, D., Maurya, M. R., Subramaniam, S. & Mercola, M. Developing microRNA screening as a functional genomics tool for disease research. *Front. Physiol.* **4,** 223 (2013).
15. Cerignoli, F. *et al.* High throughput measurement of Ca^{2+} dynamics for drug risk assessment in human stem cell-derived cardiomyocytes by kinetic image cytometry. *J. Pharmacol. Toxicol. Methods* **66,** 246–256 (2012).
16. Beuckelmann, D. J., Nabauer, M. & Erdmann, E. Intracellular calcium handling in isolated ventricular myocytes from patients with terminal heart failure. *Circulation* **85,** 1046–1055 (1992).
17. Piacentino, V. III *et al.* Cellular basis of abnormal calcium transients of failing human ventricular myocytes. *Circ. Res.* **92,** 651–658 (2003).
18. Krützfeldt, J. *et al.* Silencing of microRNAs *in vivo* with 'antagomirs'. *Nature* **438,** 685–689 (2005).
19. Bonauer, A. *et al.* MicroRNA-92a controls angiogenesis and functional recovery of ischemic tissues in mice. *Science* **324,** 1710–1713 (2009).
20. Helwak, A., Kudla, G., Dudnakova, T. & Tollervey, D. Mapping the human miRNA interactome by CLASH reveals frequent noncanonical binding. *Cell* **153,** 654–665 (2013).
21. Kho, C. *et al.* SUMO1-dependent modulation of SERCA2a in heart failure. *Nature* **477,** 601–605 (2011).
22. Kho, C., Lee, A. & Hajjar, R. J. Altered sarcoplasmic reticulum calcium cycling—targets for heart failure therapy. *Nature Rev. Cardiol.* **9,** 717–733 (2012).
23. Higazi, D. R. *et al.* Endothelin-1-stimulated InsP3-induced Ca^{2+} release is a nexus for hypertrophic signaling in cardiac myocytes. *Mol. Cell* **33,** 472–482 (2009).
24. Hulot, J. S. *et al.* Critical role for stromal interaction molecule 1 in cardiac hypertrophy. *Circulation* **124,** 796–805 (2011).
25. Fu, Y. *et al.* Regulation of NADPH oxidase activity is associated with miRNA-25-mediated NOX4 expression in experimental diabetic nephropathy. *Am. J. Nephrol.* **32,** 581–589 (2010).
26. Schmidt, H. H., Wingler, K., Kleinschnitz, C. & Dusting, G. NOX4 is a Janus-faced reactive oxygen species generating NADPH oxidase. *Circ. Res.* **111,** e15–16 (2012).
27. Dirkx, E. *et al.* Nfat and miR-25 cooperate to reactivate the transcription factor Hand2 in heart failure. *Nature Cell Biol.* **15,** 1282–1293 (2013).

Supplementary Information is available in the online version of the paper.

Acknowledgements We thank P. Aza-Blanc and F. Cerignoli; O. Kim, L. Liang and E. Kohlbrenner for their technical support; G. Christensen for providing the SERCA2a knockout mice; and H. el Azzouzi for TAC operations and histological sections. This work was supported by California Institute for Regenerative Medicine (RC1-000132), the National Institutes of Health (NIH) (R01HL113601, P01HL098053 and R01HL108176) and the Fondation Leducq to M.M.; by the NIH (NIH R01HL093183, R01HL088434, P20HL100396 and a Program of Excellence in Nanotechnology Contract no. HHSN26820100045C and P50HL112324) to R.J.H.; P30CA030199 and P30AR061303 for Sanford-Burnham Medical Research Institute functional genomics and cytometry. W.J.P. was supported by the Global Research Laboratory Program of the South Korean Government (M6-0605-00-0001). J.P.G.S. and P.A.F.D. were supported by the Netherlands Heart foundation and Project P1.05 LUST of the BioMedical Materials institute co-funded by the Dutch Ministry of Economic Affairs, Agriculture and Innovation. C.W. was supported by a fellowship from the Spanish National Research Council. A.v.M. was a Netherlands Heart Institute ICIN fellow.

Author Contributions C.W., A.R.-M., D.J., R.J.H. and M.M. conceived and designed the project following an initial concept from M.M.; C.W., D.J., A.R.-M., C.K., A.L., S.M. and A.v.M. performed experiments and analysed the data; and interpreted results with M.M. and R.J.H. W.J.P. developed reagents for post-translational modification assays on SERCA2a. M.M., R.J.H., C.W., A.R.-M., D.J., A.v.M., P.A.F.D. and J.P.G.S. wrote and edited the manuscript. Major funding was obtained by P.A.F.D., R.J.H. and M.M.

Author Information Reprints and permissions information is available at www.nature.com/reprints. The authors declare no competing financial interests. Readers are welcome to comment on the online version of the paper. Correspondence and requests for materials should be addressed to M.M. (mmercola@sanfordburnham.org).

METHODS

Cell culture. HEK293 cells were maintained in DMEM/F12 medium supplemented with 10% FBS, 100 units ml^{-1} penicillin and 100 μg ml^{-1} streptomycin. HL-1 cells were maintained in Claycomb medium (Sigma) supplemented with 10% FBS (Sigma), 100 units ml^{-1} penicillin, 100 μg ml^{-1} streptomycin, 2 mM L-glutamine, 0.1 mM noradrenaline (Sigma) and passaged approximately every 3–4 days when cells reached confluency and spontaneous contractions were observed. For transient transfection of both cell lines, Lipofectamine 2000 (Life Technologies) was used following the manufacturer's protocol. Cy3-labelled negative control siRNA (Ambion, AM4621) or miRNA (Ambion, AM17120) was used for control in all transfection experiments. Transfection efficiency was >90%.

NRVCs were isolated with the neonatal rat cardiomyocyte isolation kit (Worthington) and cultured at 37 °C with 5% CO_2. In brief, ventricles were dissected from 1–2-day-old Hsd:Sprague–Dawley rats, then digested overnight at 4 °C with trypsin. Digestion continued the following morning with collagenase for approximately 90 min at 37 °C. Cells were pooled, pre-plated for 90 min on an uncoated dish to remove fibroblasts, and transfected as above on matrigel-coated cell culture plastic dishes in high-serum media (DMEM/F12 (1:1), 0.2% BSA, 3 mM sodium-pyruvate, 0.1 mM ascorbic acid, 4 mg l^{-1} transferrin, 2 mM L-glutamine, 100 nM thyroid hormone (T3) supplemented with 10% horse serum and 5% FCS) at 2×10^5 cells cm^{-2}. After 24 h, media was changed to low-serum medium (the same but with 0.25% FCS). At 72 h cells were processed for calcium imaging (see later).

Target sensor. To screen for miRNA repression of the cardiac-specific *SERCA2a* isoform we substituted the CMV promoter of the pDsRed-N1 vector (Clontech) with the hPGK promoter driving expression of eGFP. We focused on the *SERCA2a* 3′ UTR as it is selectively expressed in cardiomyocytes (in contrast to *SERCA2b* sequences) to test the hypothesis that the cardiac-specific isoform might be under distinct regulatory control. DsRed sequence was replaced with the human *SERCA2a* 3′ UTR sequence (nucleotides 3503–4302, GenBank accession number NM_001681.3), which was obtained by PCR of differentiated human embryonic stem cells displaying spontaneous contractions. Primer sequences used for amplification were as follows: human *SERCA2a* forward: 5′-CGGGGTACCTGCAATACTGGAGTAACCGCTTC-3′; human *SERCA2a* reverse: 5′-CGGCGGCCGCATTTACCTGAAACCATGTCTGTGC-3′.

miRNA screen. HEK293 cells were co-transfected with the Ambion Pre-miR miRNA Precursor Human v.2.0 microRNA library and 300 ng *SERCA2a* 3′ UTR target sensor plasmid per well in 384-well plates (Greiner). Transfections were performed using Lipofectamine 2000 (Life Technologies) in triplicate with 25 nM of each miRNA. At 48 h after transfection cells were fixed in 4% paraformaldehyde and imaging was performed using an automated fluorescent microscope (InCell Analyzer 1000; GE Healthcare) and analysed using CyteSeer software (Vala Sciences) by quantifying Total Integrated Pixel Intensity within an eGFP-positive area, as described[28,29]. Hits were confirmed by a 5-point dose response assay (50 nM to 3.125 nM), and data plotted (Fig. 1e) as the AUC. Thirty-two were determined to be evolutionarily conserved between mouse and human (TargetScan v.6.2), and 15 were both evolutionarily conserved and reported to be upregulated in human heart failure[4,5,30–36].

Site-directed mutagenesis. Site-directed mutagenesis was used to modify the *miR-25* seed binding sequence using Pfu Turbo DNA Polymerase. DpnI was used to digest non-mutated DNA template before transforming the mutated plasmids. Primers used were as follows: *SERCA2a* 3′ UTR forward: 5′-GCAGTAGACAGATGTTG**TTCGAA**TACAAATATTGTGATGC-3′; *SERCA2a* 3′ UTR reverse: 5′-GCATCACAATATTTGTA**TTCGAA**CAACATGTGTCTACTGC-3′; *IP3R1* 3′ UTR forward: 5′-ATGTTTTTTATAAAACT**CATATG**TACGAATTATGCAATCAC-3′; *IP3R1* 3′ UTR reverse: 5′-GTGATTGCATAATTCGTA**CATATG**AGTTTTATAAAAAACAT-3′.

The mutated sequences were designed to contain restriction enzyme recognition sites (highlighted in bold), used to verify correct mutation of the seed site.

IP3R1 target sensor luciferase assay. HEK293 cells were co-transfected with miRNA (25 nM) and 100 ng human IP3R Type 1 miTarget (GeneCopoeia). Forty-eight hours after transfection, reporter activity was analysed using the Dual-Glo Luciferase Assay System (Promega) and EnVision plate reader (PerkinElmer). Data are presented as a ratio of firefly luciferase activity normalized to *Renilla* luciferase.

RT–qPCR. RNA was isolated from human tissue using Trizol (Life Technologies) according to the manufacturer's protocol. All-in-One miRNA qRT–PCR Detection Kit (GeneCopoeia) was used for both cDNA synthesis and quantitative detection using *miR-25*-specific primers (GeneCopoeia). *Rnu6* was used for normalization.

RNA was isolated from mouse tissue using mirVana miRNA Isolation kit (Life Technologies) according to the manufacturer's protocol. The TaqMan MicroRNA Assays kit (Life Technologies) was used for both cDNA synthesis and qPCR using *miR-25* primers (Life Technologies). *miR-24* was used for normalization.

***In situ* hybridization.** To characterize the distribution and cellular origin of *miR-25* in heart failure we performed *in situ* hybridization on 10 μm-thick cryosections of TAC-induced heart failure mice (1 month post-TAC). Sections were fixed by 4% paraformaldehyde for 10 min, acetylated for 10 min and permeabilized for 5 min by proteinase K treatment (5 μ ml^{-1}). Prehybridization of sections was performed for 4 h at RNA melting temperature (T_m) minus 30 °C (specific for each LNA probe) before overnight hybridization with 25 nM 5′-DIG- and 3′-DIG-labelled miRCURY LNA miRNA detection probes (Exiqon) for *miR-25* (18122-15), negative control *miR-159* (99003-15) and positive control U6 (99002-15) at T_m minus 30 °C in denaturizing hybridization buffer. To remove unbound and partially bound probes slides were washed for 15 min in 5× SSC and for 1 h in 0.2× SSC at 60 °C. After washing, sections were blocked for 1 h before overnight incubation at 4 °C with anti-DIG alkaline phosphatase antibody (1:1,500, Roche). For miRNA visualization, sections were subsequently incubated in Liquid Permanent Red (Dako) for 6 h. Co-staining for the non-cardiomyocyte fraction was performed by incubation with lectin BS-1 (1:100, Sigma), anti-α-SMA (1:400, Sigma), or periostin (1:50, Sigma) for 1 h at room temperature (22 °C), followed by 1 h incubation with appropriate Alexa Fluor 488 secondary antibodies (Life Technologies). Hoechst 33342 (Life Technologies) was used as a counterstain and slides were mounted in Fluoromount G (SouthernBiotech). Images were captured using cellP software (Olympus) on an Olympus BX60 microscope and processed with Adobe Photoshop Cs4 v.11.

Protein expression analyses. For *in vitro* transfection experiments using HL-1 cells, cells were transfected with miRNAs (50 nM), and samples were lysed 72 h later using Novex Tris-Glycine 2× Sample Buffer supplemented with 5% β-mercaptoethanol at 55 °C for 1 h. Samples were loaded on SDS–PAGE gels for separation, followed by blotting of protein onto polyvinylidene fluoride membrane. Membranes were then incubated as follows: SERCA2a (1:2,000; 21st Century Biochemicals), IP3R1 (1:200, goat polyclonal, sc-6093; Santa Cruz Biotechnology), calmodulin (1:2,000, rabbit monoclonal, ab45689; Abcam), NCX1 (1:500, mouse monoclonal, MAB1590; Chemicon), GAPDH (1:1,000, rabbit polyclonoal, ab9485; Abcam), phosopholamban (1:500, mouse monoclonal, 05-205; Upstate) and CaMKII (1:10,000, gift from J. H. Brown laboratory). AlexaFluor-labelled secondary antibodies were used (1:10,000) for detection of the specific bands. Quantitative analysis was done using the Odyssey imaging system (LI-COR Biosciences).

Calcium imaging and analysis. HL-1 cells were seeded at a density of 25,000 cells per well on 96-well glass-bottom plates (Greiner) and transfected with 50 nM miRNAs as described for cell culture earlier. NRVCs were seeded at a density of 60,000 cells per well, and were processed identically, with the addition of a single 15 V electrical pulse of 5 ms at 1 Hz, initiated at 2 s into recording.

Seventy-two hours after transfection, cells were loaded with 200 ng ml^{-1} Hoechst 33342 (Sigma) and Fluo-4 for 30 min at 37 °C followed by 30 min at room temperature. Fluo-4 NW Calcium Assay Kit (Life Technologies) was prepared according to the manufacturer's instructions in 1× Hanks Balanced Salt Solution containing 20 mM HEPES buffer (Life Technologies) and 2.5 mM Probenecid (Life Technologies). After loading, cells were incubated with Tyrode's solution (140 mM NaCl, 6 mM KCl, 1 mM $MgCl_2$, 5 mM HEPES, 2 mM $CaCl_2$, 10 mM glucose, pH 7.4) for imaging. Ca^{2+} transient recordings were done using a Kinetic Image Cytometer IC 100 (Vala Sciences). Video streams of 10 s of the Fluo-4 green channel were collected for each well at 33 frames per second. Autofocus by the IC 100 was performed automatically by video acquisition using the nuclear channel. All image capture was performed with a ×20 0.50 numerical aperture (NA) objective. Cytometric calcium kinetic parameters were determined by image analysis using CyteSeer software (Vala Sciences) and unresponsive or low responding cells were removed by gating.

Bioinformatics. Predicted *miR-25* target binding sites were obtained from TargetScan Human v.6.2 (http://www.targetscan.org). Potential targets of *miR-25* involved in calcium signalling pathways were identified using DianaLab miRPath with TargetScan Mouse v.5.0 prediction software (http://diana.cslab.ece.ntua.gr/pathways).

AAV9 transduction. AAV9-*miR-25* and AAV9-*miR-92a* were produced using the two-plasmids protocol described previously[37] with the following modifications: 293-T cells (ATCC) were grown in triple flasks for 24 h (DMEM, 10% FBS) before the transfection using polyethyleneimine (PEI). After 72 h, cells were harvested and only DNase resistant virus was purified by an iodixanol density gradient (Optiprep; Greiner Bio-One). Finally, viruses were concentrated and formulated into lactated Ringer's solution (Baxter Healthcare Corporation) using a Vivaspin 20 Centrifugal concentrator 100K MWCO (Vivascience) and stored at −80 °C. On the day of the injection, mice were immobilized using the single mouse restrainer (Harvard apparatus) and the indicated amount (5×10^{11} vector genomes (vg) per mouse) of AAV9 was injected through the tail vein.

AAV transduction of *miR-25* and *miR-92a* yielded a comparable copy number (Extended Data Fig. 5). To quantify *miR-25* and *miR-92a* copy number in mice, we used a SYBR green-based real-time quantitative assay. Genomic AAV9-*miR-25* and *miR-92a* vector DNA was extracted from frozen cardiac tissues by using DNeasy Tissue Kits (Qiagen). The real-time qPCR assay detects a 145-bp sequence

unique to the SV40 promoter in the AAV9 vector (forward: TTGGACAAACCA CAACTAGAA; reverse: AACCTCCCACACCTCCC). Genomic DNA was isolated from the indicated tissues and 100 ng of each sample was used in duplicate to determine vector genome copies. The plasmid DNA was used as a copy number standard ranging from 10 to 10^8 copies μl^{-1}. The lower limit detection of the assay was 150 copies μg^{-1} DNA.

TAC surgery. Male mice (B6C3F1 strain) of 8–10 weeks of age (25–30 g) were used. The animals were anaesthetized with ketamine (95 mg kg^{-1}) and xylazine (5 mg kg^{-1}) administered via intraperitoneal injection. The mice were ventilated with a tidal volume of 0.1 ml and a respiratory rate of 110 breaths per minute (Harvard Apparatus). A longitudinal incision of 2–3 mm was made in the proximal sternum to allow visualization of the aortic arch. The transverse aortic arch was ligated between the innominate and left common carotid arteries with an overlaid 27-gauge needle. The needle was then immediately removed, leaving a discrete region of constriction. Echocardiography was performed and Doppler was used to calculate the pressure gradient between proximal and distal sites of the transverse aortic constriction. Only animals with a pressure gradient >30 mm Hg were included in this study. After 8 weeks, additional echocardiography was performed to evaluate cardiac function. Only animals with FS $< 50\%$ were determined as being in heart failure and suitable for further study.

Anti-miRNA administration. Anti-*miR-25* (product code AM10584), anti-miRNA negative control (product code AM17010) were purchased from Ambion. Separate solutions of anti-*miR-25* and anti-miRNA negative control were each diluted with *in vivo*-jetPEI solution (catalogue no. 201-50, Polyplus-transfection) containing 10% (wt/vol) glucose at a ratio of *in vivo*-jetPEI nitrogen residues per oligonucleotide phosphate of 5, following the recommendations of the manufacturer. All solutions were mixed by vortexing for 10 s and incubated for at least 15 min at 37 °C before injection. Each mouse received 400 µl saline and oligonucleotide mixture (100 µl of oligonucleotide solution plus 300 µl of saline, corresponding to 300 µg of oligonucleotide per dose) through tail vein injection consecutively for 3 days and 3 additional injections were performed once a week for the following 3 weeks. Two additional groups of control animals were included: one consisting of untreated animals and the other of animals receiving a mixture of *in vivo*-jetPEI solution containing 10% (wt/vol) glucose without added oligonucleotide. All injections were carried out using a 30-gauge needle syringe with single mouse restrainer (Harvard apparatus).

Production of SERCA2a knockout mice. Conditional SERCA2 knockout mice were donated by G. Christensen[38]. The mice were generated by standard gene targeting strategies to introduce loxP sites into introns 1 and 3 of the *Serca2*. For our studies, 8–10-week-old mice were injected intraperitoneally with 4-OH-tamoxifen (1 mg per day) for 4 days to induce cardiomyocyte-specific excision of the *Serca2* gene sequences, essentially as described[38,39].

Echocardiography and *in vivo* haemodynamics. B6C3F1 mice were acquired from Jackson laboratories. Mice were anaesthetized with intraperitoneal ketamine (100 µg g^{-1}) for echocardiographic analysis. Two-dimensional images and M-mode tracings were recorded on the short-axis at the level of the papillary muscle to determine percent fractional shortening and ventricular dimensions (GE Vivid Vision). One day after echocardiography, *in vivo* haemodynamics were performed using a 1.2 Fr pressure–volume (PV) conductance catheter (Scisense). Mice were anaesthetized with an intraperitoneal injection mixture of urethane (1 mg g^{-1}), etomidate (10 µg g^{-1}) and morphine (1 µg g^{-1}) and were then intubated via a tracheotomy and mechanically ventilated at 7 µl g^{-1} tidal volume and 120 respirations per minute. The PV catheter was placed in the LV via an apical stab approach as previously described[40]. Pressure–volume data were analysed using IOX2 software (EMKA technologies). All procedures were approved by and performed in accordance with the Institutional Animal Care and Use Committee of the Mount Sinai School of Medicine. The investigation conforms with the Guide for the Care and Use of Laboratory Animals published by the US National Institutes of Health (NIH publication no. 85–23, revised 1996).

Histological examination of cardiac tissues. To measure cardiomyocyte cross-sectional area, suitable cross-sections with nearly circular capillary profiles and nuclei were selected on sections stained with WGA followed by a fluorescein isothiocyanate (FITC)-conjugated rabbit polyclonal to WGA (1:100; ab20528, Abcam). These were observed using an Axiophot microscope (Carl Zeiss), and then analysed using the Analysis-SIS3.2 software (Soft-Imaging System). To measure the fibrotic areas, a Masson-trichrome staining kit (Sigma-Aldrich; HT15-1kt) was used for staining of the sectioned hearts. The fibrotic areas stained blue and the normal tissue stained red. The fibrotic area was calculated as the ratio of the total area of fibrosis to the total area of the section.

Statistical analysis. Data are presented as mean $\pm$ s.e.m.. Unpaired Student's *t*-test or ANOVA was performed as indicated to determine statistical differences. Whisker box plots show outliers beyond the 5th and 95th percentiles. All statistical analyses were done using GraphPad Prism software.

28. Colas, A. R. *et al.* Whole-genome microRNA screening identifies let-7 and mir-18 as regulators of germ layer formation during early embryogenesis. *Genes Dev.* **26,** 2567–2579 (2012).
29. McKeithan, W. L., Colas, A. R., Bushway, P. J., Ray, S. & Mercola, M. Serum-free generation of multipotent mesoderm (Kdr^+) progenitor cells in mouse embryonic stem cells for functional genomics screening. *Curr. Protoc. Stem Cell Biol.* Chapter 1, 13 (2012).
30. Roy, S. *et al.* MicroRNA expression in response to murine myocardial infarction: miR-21 regulates fibroblast metalloprotease-2 via phosphatase and tensin homologue. *Cardiovasc. Res.* **82,** 21–29 (2009).
31. Matkovich, S. J. *et al.* Reciprocal regulation of myocardial microRNAs and messenger RNA in human cardiomyopathy and reversal of the microRNA signature by biomechanical support. *Circulation* **119,** 1263–1271 (2009).
32. van Rooij, E. *et al.* Dysregulation of microRNAs after myocardial infarction reveals a role of miR-29 in cardiac fibrosis. *Proc. Natl Acad. Sci. USA* **105,** 13027–13032 (2008).
33. Cheng, Y. *et al.* MicroRNAs are aberrantly expressed in hypertrophic heart: do they play a role in cardiac hypertrophy? *Am. J. Pathol.* **170,** 1831–1840 (2007).
34. Tatsuguchi, M. *et al.* Expression of microRNAs is dynamically regulated during cardiomyocyte hypertrophy. *J. Mol. Cell. Cardiol.* **42,** 1137–1141 (2007).
35. Sayed, D., Hong, C., Chen, I. Y., Lypowy, J. & Abdellatif, M. MicroRNAs play an essential role in the development of cardiac hypertrophy. *Circ. Res.* **100,** 416–424 (2007).
36. van Rooij, E. *et al.* A signature pattern of stress-responsive microRNAs that can evoke cardiac hypertrophy and heart failure. *Proc. Natl Acad. Sci. USA* **103,** 18255–18260 (2006).
37. Zolotukhin, S. *et al.* Recombinant adeno-associated virus purification using novel methods improves infectious titer and yield. *Gene Ther.* **6,** 973–985 (1999).
38. Andersson, K. B. *et al.* Moderate heart dysfunction in mice with inducible cardiomyocyte-specific excision of the *Serca2* gene. *J. Mol. Cell. Cardiol.* **47,** 180–187 (2009).
39. Swift, F. *et al.* Extreme sarcoplasmic reticulum volume loss and compensatory T-tubule remodeling after *Serca2* knockout. *Proc. Natl Acad. Sci. USA* **109,** 3997–4001 (2012).
40. Pacher, P., Nagayama, T., Mukhopadhyay, P., Batkai, S. & Kass, D. A. Measurement of cardiac function using pressure–volume conductance catheter technique in mice and rats. *Nature Protocols* **3,** 1422–1434 (2008).
41. Bers, D. M. Calcium cycling and signaling in cardiac myocytes. *Annu. Rev. Physiol.* **70,** 23–49 (2008).
42. Kockskämper, J. *et al.* Emerging roles of inositol 1,4,5-trisphosphate signaling in cardiac myocytes. *J. Mol. Cell. Cardiol.* **45,** 128–147 (2008).
43. Bootman, M. D. & Roderick, H. L. Why, where, and when do cardiac myocytes express inositol 1,4,5-trisphosphate receptors? *Am. J. Physiol. Heart Circ. Physiol.* **294,** H579–H581 (2008).
44. Zima, A. V., Bare, D. J., Mignery, G. A. & Blatter, L. A. IP3-dependent nuclear Ca^{2+} signalling in the mammalian heart. *J. Physiol. (Lond.)* **584,** 601–611 (2007).

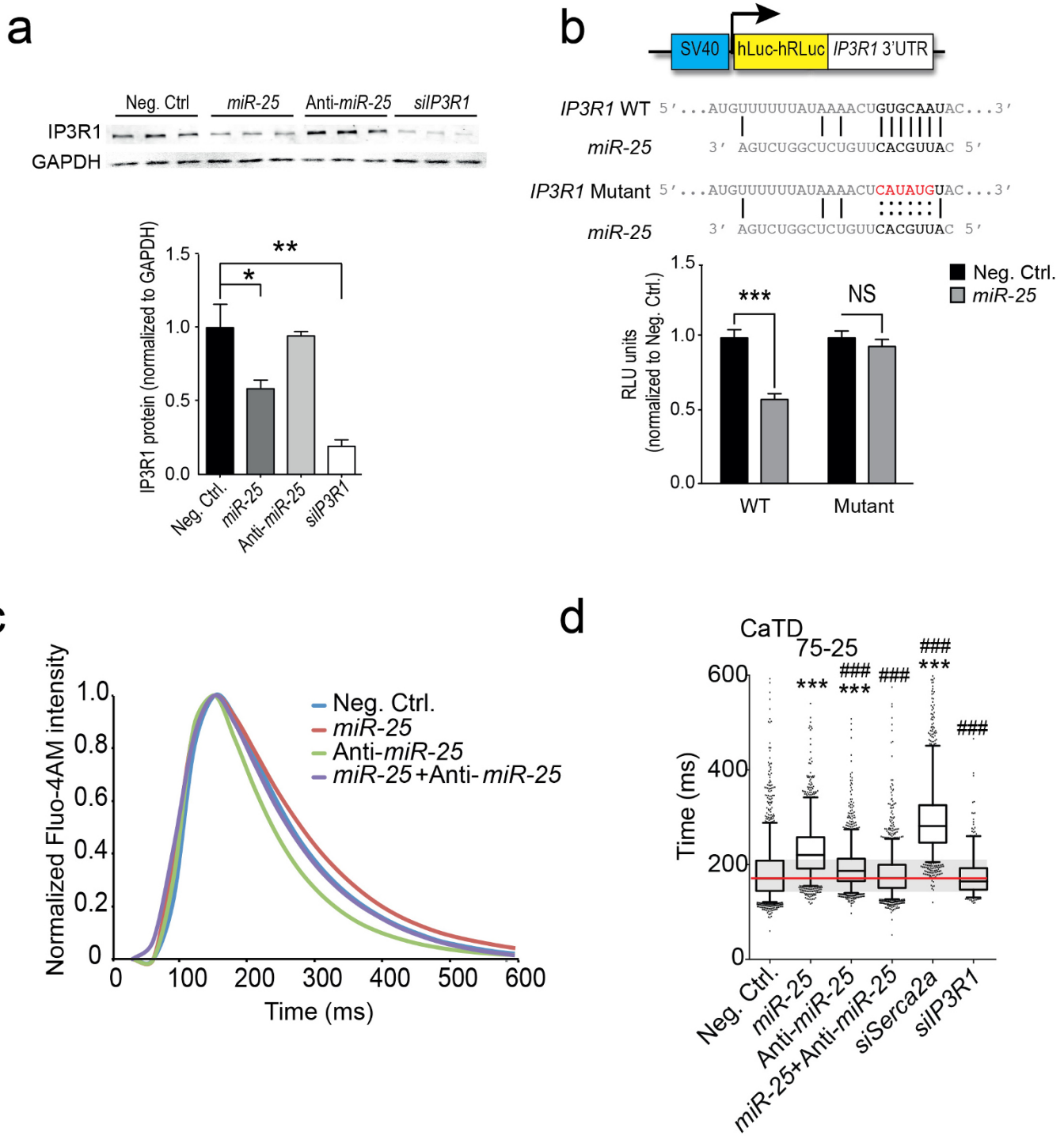

Extended Data Figure 1 | Effect of *miR-25* on IP3R1 and cardiomyocyte calcium transients *in vitro*. **a**, Effect of *miR-25*, anti-*miR-25* and *siIP3R1* transfection on IP3R1 protein levels in HL-1 cells. **b**, Sequence of the putative *miR-25* target recognition element in *IP3R1* mRNA and the corresponding alteration by site-directed mutagenesis. Mutation abolished inhibition of the luciferase signal by *miR-25* ($n = 10$). **a**, **b**, Data are represented as mean ± s.e.m. $^{*}P < 0.05$, $^{**}P < 0.01$, $^{***}P < 0.001$. NS, not significant (Student's *t*-test). **c**, Representative Ca^{2+} transient of HL-1 cells transfected as indicated. Note that *miR-25* slowed the repolarization phase kinetics, whereas anti-*miR-25* quickened the kinetics. Co-transfection normalized kinetics. **d**, Kinetic imaging cytometry analysis of Ca^{2+} transient kinetics during the decay phase (Ca^{2+} transient duration time from 75% to 25% maximal value, $CaTD_{75-25}$) of transfected NRVCs ($n > 550$ cells). Box defines interquartile range; bar shows median; whiskers show ± 5th and 95th percentile; dots indicate outliers. $^{*}P < 0.05$, $^{**}P < 0.01$, $^{***}P < 0.001$. NS, not significant (one-tailed ANOVA). Experiments were replicated two times.

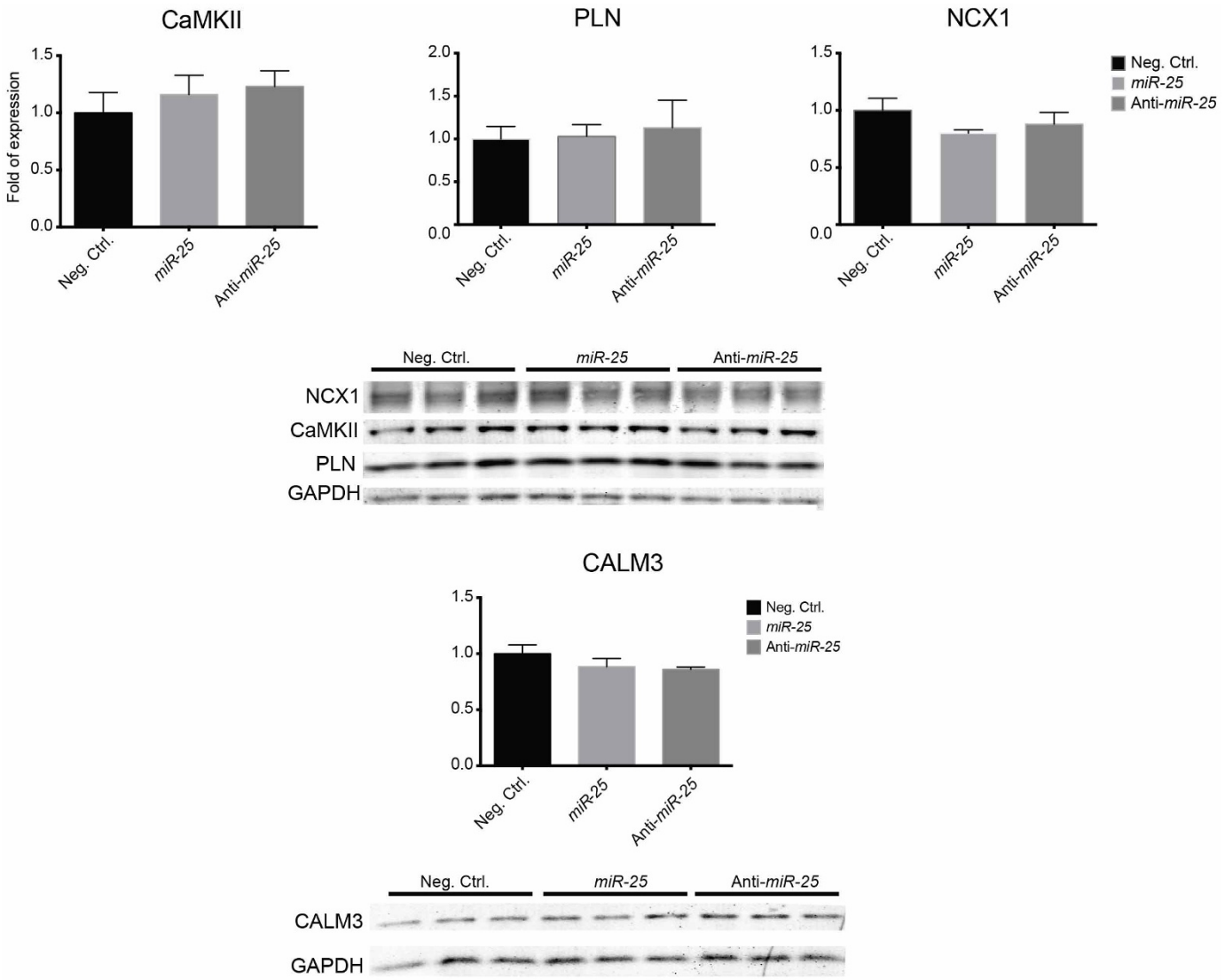

Extended Data Figure 2 | Effect of *miR-25* on calcium handling proteins. Expression of candidate targets of *miR-25* in transfected HL-1 cells (lysates collected 5 days post-transfection). No effect of *miR-25* or *anti-miR-25* was noted for these proteins. Data are represented as mean ± s.e.m. Experiments were replicated two times.

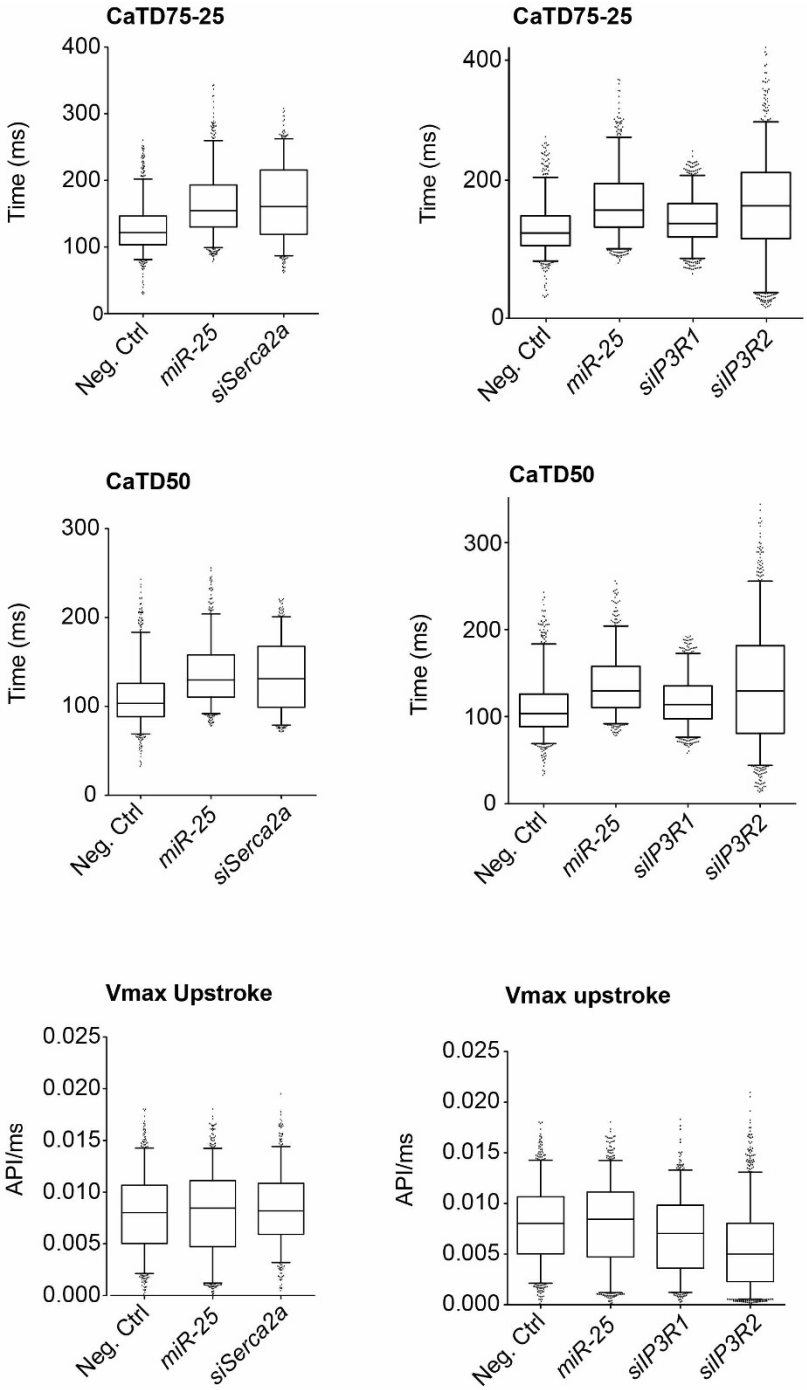

Extended Data Figure 3 | Calcium transient effects of *miR-25* compared with that of siRNAs against SERCA2a and IP3R isoforms. Cardiomyocyte-like HL-1 cells were transfected with *miR-25*, siRNA to SERCA2a (*siSerca2a*) (left panels) or siRNAs to IP3R1 or IP3R2 (*siIP3R1*, *siIP3R2*) (right panels), and analysed 72 h later by kinetic imaging cytometry. Kinetic parameters are $CaTD_{50}$, $CaTD_{75-25}$ and V_{max} upstroke. Data are represented as whisker plots, with the box denoting the 25th and 75th percentiles, the whiskers the 5th and 95th percentiles, the middle bar the median, and outliers indicated as individual dots. Note that *siSerca2a* and *miR-25* elicited comparable effects, both markedly delaying the Ca^{2+} uptake phase parameters $CaTD_{50}$ and $CaTD_{75-25}$ without appreciably altering the V_{max} upstroke kinetics ($n > 550$ cells per group). Box defines interquartile range; whiskers indicate ± 5th and 95th percentile; dots indicate outliers. Also note that *siIP3R1* only minimally affected the Ca^{2+} kinetic parameters. *siIP3R2* slowed V_{max} upstroke and broadened the distribution of uptake phase kinetic parameters $CaTD_{50}$ and $CaTD_{75-25}$. *miR-25* in contrast slowed the uptake phase parameters but did not appreciably affect V_{max} upstroke ($n > 550$ cells per group). Box defines interquartile range; whiskers indicate ± 5th and 95th percentile; dots indicate outliers. Although IP3R1 might be a direct target of *miR-25*, several lines of evidence suggest that it is unlikely to mediate the effect of *miR-25* in heart failure. IP3Rs are intracellular ligand-gated Ca^{2+} release channels[41] that in the sarcoplasmic reticulum are associated with excitation–contraction coupling or spontaneous Ca^{2+} release and enhanced Ca^{2+} transients, whereas in the nuclear envelope they promote nuclear Ca^{2+} signalling[42–44], but a specific role for IP3R1 in heart failure has not been identified. Nonetheless, the control of IP3R1 by *miR-25* might have a critical role under conditions that sensitize cardiomyocytes to inositol-1,4,5-trisphosphate, such as in response to endothelin 1, angiotensin and phenylephrine[23] or in local Ca^{2+} control[24]. Experiments were replicated two times.

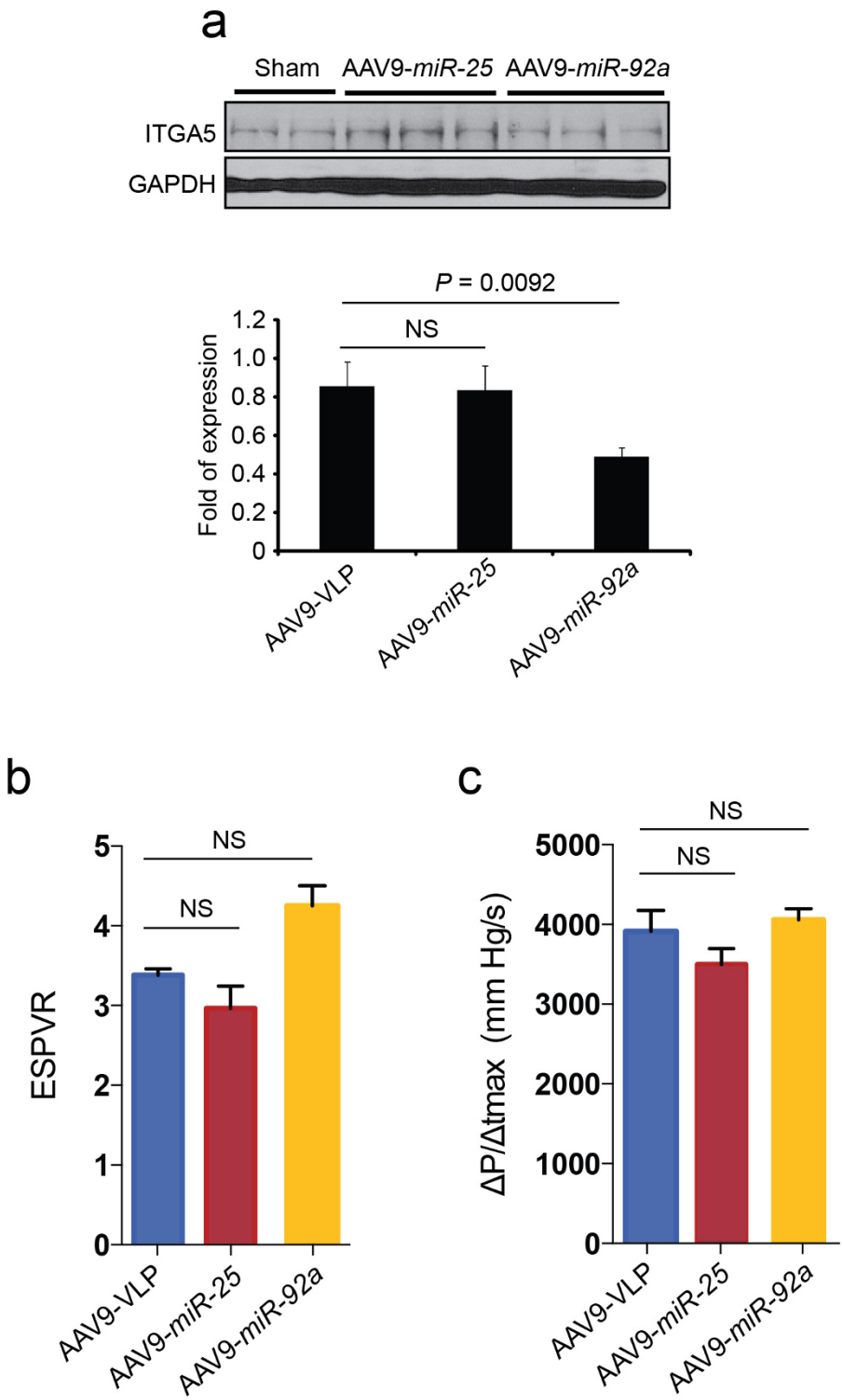

Extended Data Figure 4 | Effect of *miR-25* and *miR-92a* overexpression *in vivo*. **a**, Effect of AAV9-mediated cardiac gene transfer of *miR-25* and *miR-92a* on target protein levels. Cardiac gene transfer of *miR-25* and *miR-92a* increased levels of their respective miRNAs but *miR-92a* was selective against confirmed target integrin subunit α5 (ITGA5). **b**, **c**, Effects of AAV9-mediated cardiac gene transfer of *miR-25* and *miR-92a* on cardiac function. There is a tendency towards decreased cardiac function in both ESPVR (**b**) and $\Delta P/\Delta t_{max}$ (**c**) in AAV9-*miR-25*-treated animals relative to control- (AAV9-VLP) and AAV9-*miR-92a*-treated animals. n = number of biological replicates (all included): $n = 5$ (AAV9-VLP); 4 (AAV9-*miR-25*); 5 (AAV9-*miR-92a*) for panels **b**, **c**. Data are represented as mean ± s.e.m. NS, not significant.

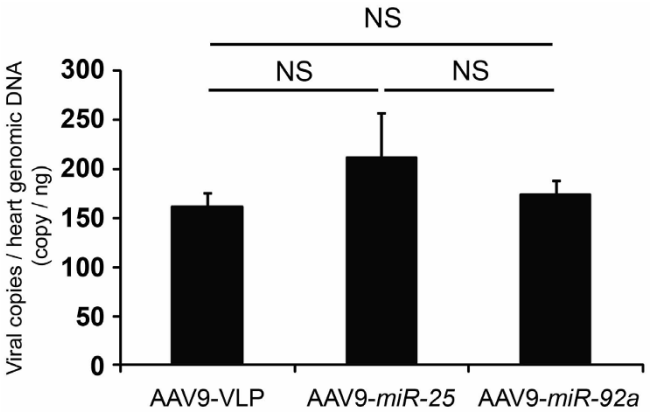

Extended Data Figure 5 | AAV9-mediated gene transfer integration in ventricular myocardium. The number of integrated *miR-25* and *miR-92a* copies in ventricular myocardium 6 weeks after AAV-mediated gene transfer, determined by qPCR (see Methods). n = number of biological replicates (all included): $n = 5$ (AAV9-VLP), $n = 4$ (AAV9-*miR-25*) and $n = 5$ (AAV9-*miR-92a*). Data are represented as mean ± s.e.m. NS, not significant.

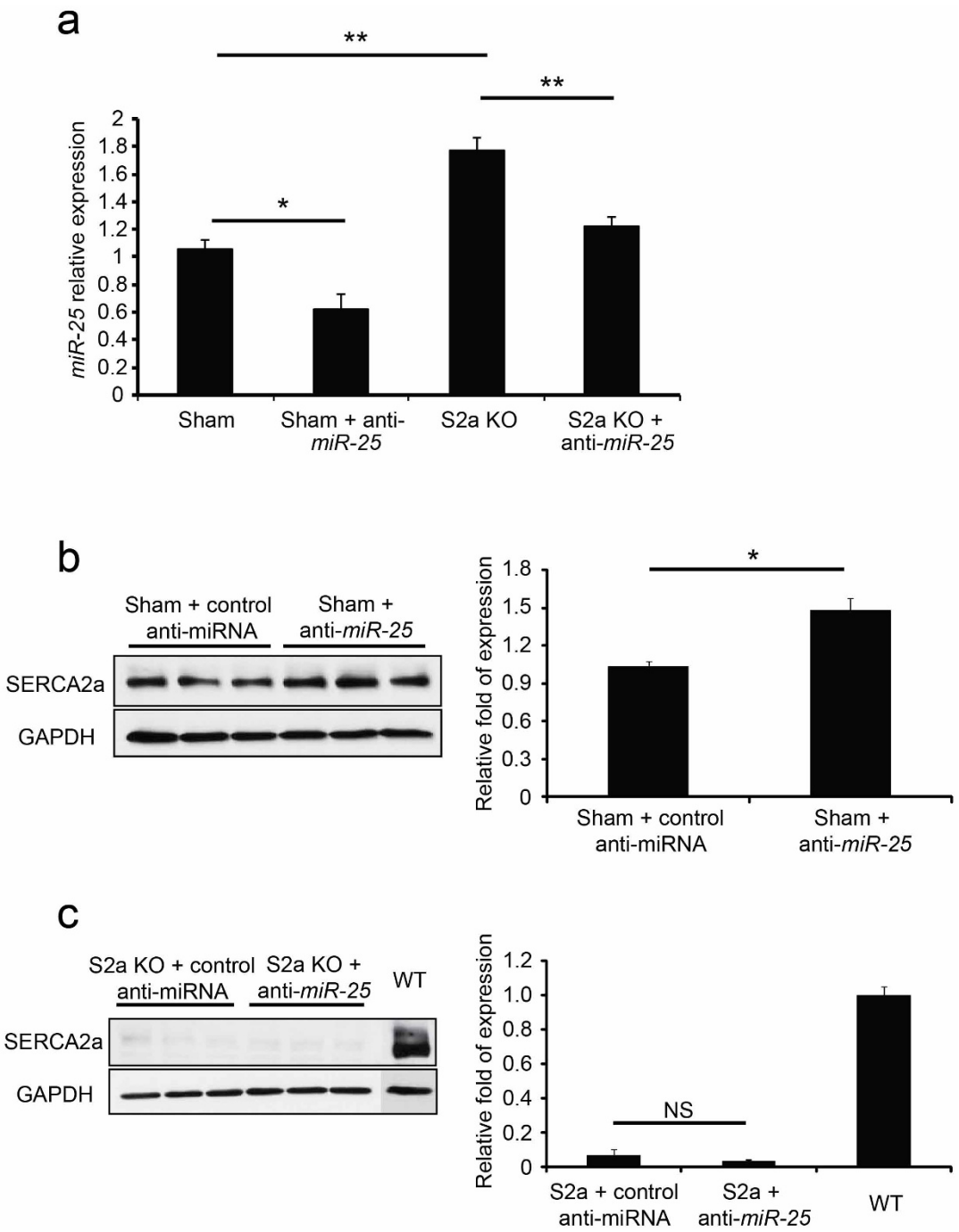

Extended Data Figure 6 | Effects of anti-*miR-25* on endogenous *miR-25* and SERCA2a in wild-type and *Serca2a*-null hearts. **a**–**c**, Anti-*miR-25* or control (scrambled sequence) anti-miRNA was administered intravenously to sham-operated wild-type mice (Sham) or to unoperated *Serca2a*-cardiomyocyte null (S2a KO) mice[38], as for the experiments in Fig. 4 (see Methods). **a**, Sham-operated animals were injected with anti-miRNAs 1 week after surgery and analysed at 4 weeks. S2a KO animals were injected with 4-OH tamoxifen intraperitoneally for 4 days to delete *Serca2a* (see Methods), injected with anti-miRNAs 1 week later and analysed 4 weeks later (5 weeks from initial 4-OH-tamoxifen injection). Note that anti-*miR-25* decreased endogenous *miR-25* levels in sham-operated wild-type and S2a KO mice relative to control-treated animals ($n = 3$). **b**, Furthermore, SERCA2a protein levels increased in the anti-*miR-25* treated wild-type animals relative to control ($n = 3$). **c**, SERCA2a is absent in S2a KO hearts. WT, wild type. In all panels data are represented as mean ± s.e.m. NS, not significant. n = number of biological replicates (all included).

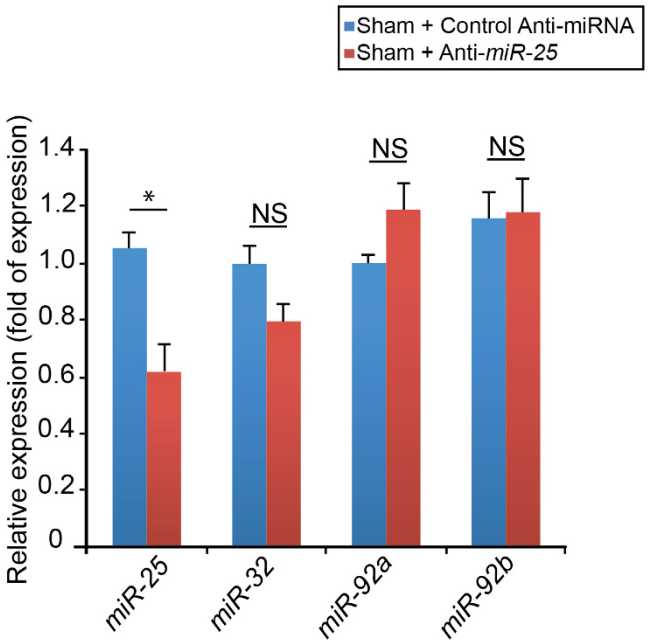

Extended Data Figure 7 | Selectivity of anti-*miR-25* on *miR-25* family. Expression levels of *miR-25* and family members (*miR-32*, *miR-92a* and *miR-92b*) in sham-operated mice that had been injected with anti-*miR-25* or control (scrambled sequence) anti-miRNA as in Fig. 4 (see Methods) ($n = 3$). n = number of biological replicates (all included). Note that control anti-miRNA in sham-operated animals did not alter expression of any of the miRNAs tested (blue bars). In contrast, anti-*miR-25* significantly reduced levels of *miR-25* but not other family members in sham-operated animals (red bars). Data are represented as mean ± s.e.m. NS, not significant.

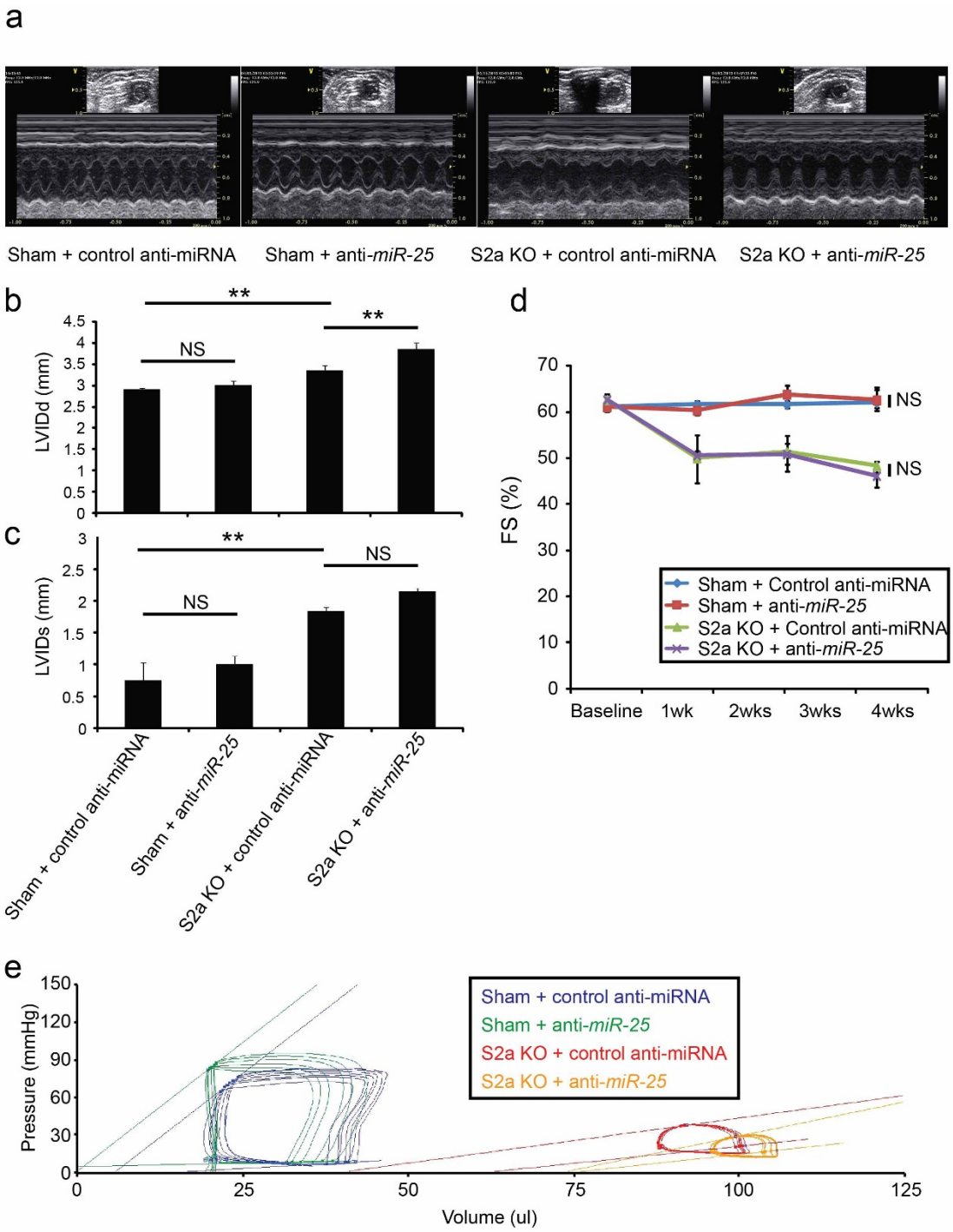

Extended Data Figure 8 | Effects of anti-*miR-25* on cardiac function of WT and *Serca2a*-null hearts. **a**–**e**, Anti-*miR-25* or control (scrambled sequence) anti-miRNA was administered intravenously to sham-operated wild-type mice (Sham) or to unoperated *Serca2a*-cardiomyocyte null (S2a KO) mice[38], as for the experiments in Fig. 4 (see Methods). Sham-operated animals were injected with anti-miRNAs 1 week after surgery and followed by echocardiography. S2a KO animals were generated by injection with 4-OH tamoxifen intraperitoneally for 4 days (see Methods) to delete *Serca2a*, then injected with anti-miRNAs 1 week later and followed by echocardiography. **a**, Representative two-dimensional guided M-mode images of the LVs from wild-type and S2a KO mice. **b**, **c**, Echocardiographic indices of left ventricular inner dimension during diastole, LVIDd (**b**), and systole, LVIDs (**c**) ($n = 3$ (sham plus control); 8, (sham plus anti-*miR-25*); 7 (S2a KO plus control); 11 (S2a-KO plus anti-*miR-25*) 4 weeks after control or anti-miRNA injection. **d**, Echocardiographic measurement of fractional shortening (FS) expressed as a percentage at time points after control or anti-miRNA injection ($n = 4$ (sham plus control); 3 (sham plus anti-*miR-25*); 3 (S2a KO plus control); 3 (S2a KO plus anti-*miR-25*)). S2a KO mice show characteristic dilation and decline in cardiac function after 4-OH tamoxifen-induced excision of *Serca2a*[39]. ***$P < 0.001$ (Student's *t*-test for difference between S2a KO and sham-operated control anti-miRNA groups at week 4 after injection). **e**, Haemodynamic effect of anti-*miR-25* and control anti-miRNA injection is represented by pressure–volume plots of treatment cohorts as indicated 4 weeks after injection of control or anti-miRNA. Note that specific anti-*miR-25* and control anti-miRNA acted similarly in sham-operated wild-type animals ($n = 3$ (sham plus control); 3, (sham plus anti-*miR-25*); 2 (S2a KO plus control); 3 (S2a-KO plus anti-*miR-25*). Moreover, anti-*miR-25* did not increase cardiac function of S2a KO mice, unlike TAC-operated wild-type mice (Fig. 4), suggesting that the beneficial effect on cardiac function depends on SERCA2a. Data are represented as mean ± s.e.m. n = number of biological replicates (all included). NS, not significant.

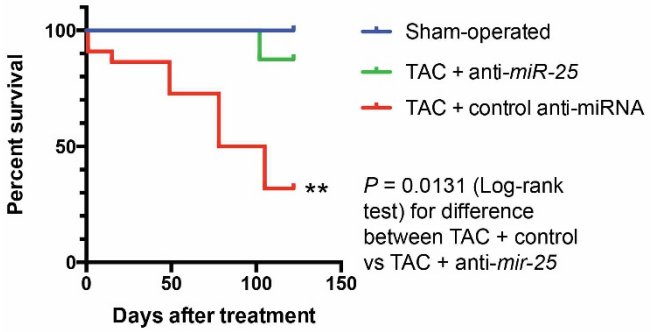

Extended Data Figure 9 | Kaplan–Meier survival curve for anti-*miR-25* treatment. Survival probability is plotted over time, showing a cumulative protective effect of anti-*miR-25* relative to control (scrambled sequence) anti-miRNA injections after TAC. The summary of two experiments is shown, plotting time from injection. Groups were sham-operated ($n = 8$), TAC plus anti-*miR-25* ($n = 8$) and TAC plus control (scrambled sequence) anti-miRNA ($n = 22$). Note that injection with specific anti-*miR-25* increased survival ($P = 0.0131$, log-rank test) relative to TAC plus control miRNA.

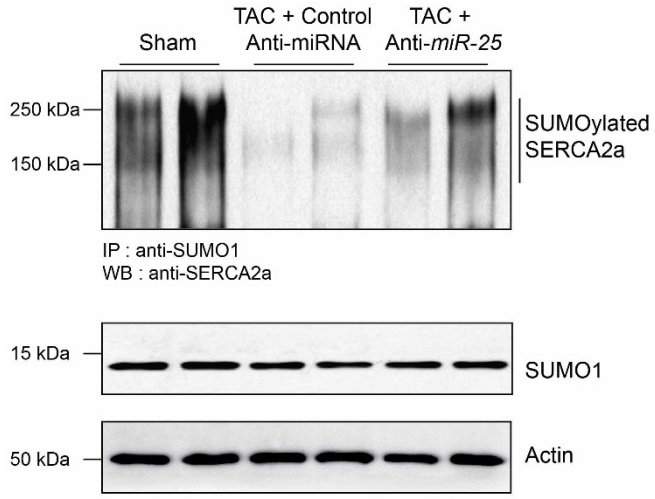

Extended Data Figure 10 | Effect of anti-*miR-25* on accumulation of SUMOylated SERCA2a. Immunoblots of lysates from heart tissue at termination of the *in vivo* study shown in Fig. 4 (5.5 months after TAC, corresponding to 3.5 months after injection of anti-*miR-25* or control (scrambled sequence) anti-miRNA). Lysates were immunoprecipitated with anti-SUMO1 followed by western blotting with anti-SERCA2a, as described previously[21]. Experiments were replicated three times. Note the reduction in SUMOylated SERCA2a upon TAC in the control anti-miRNA treated hearts, but restoration of expression after specific anti-*miR-25* injection. Total levels of SUMO1 and actin are shown.